Supplementary Information

Gradient Control of the Adhesive Force between Ti/TiO_2 Nanotubular Arrays fabricated by anodization

Minghui Zhao, Jidong Li, Yubao Li, Jian Wang, Yi Zuo, Jiaxing Jiang and Huanan Wang*

Research Center for Nano-Biomaterials, Analytical & Testing Center and State Key Laboratory of Biotherapy West China Medical School, Sichuan University, Chengdu, 610064, China

Corresponding author: E-mail: nic1979@scu.edu.cn (J.L.)

Contents:

1. Revetest Scratch Tests of specimens treated in different pure organic solvents.

Table S1. Scratch Tests of specimens treated in different pure organic solvents.

Solvent	Solvent polarity	Average Loading Force (N)	Deviation
Petroleum ether	0.01	58	10.06
Cyclohexane	0.1	48	15.62
Totuene	2.4	33	8.33
n-butyl alcohol	3.7	24	6.66
isopropyl alcohol	4.3	15	13.65
acetone	5.4	27	3.51
methyl alcohol	6.6	0	0
DMSO	7.2	26	6.51
H_2O		20	3.21

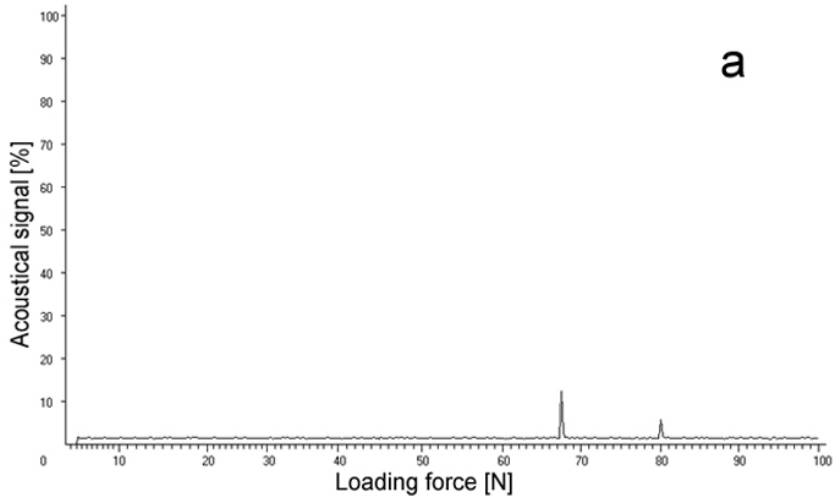

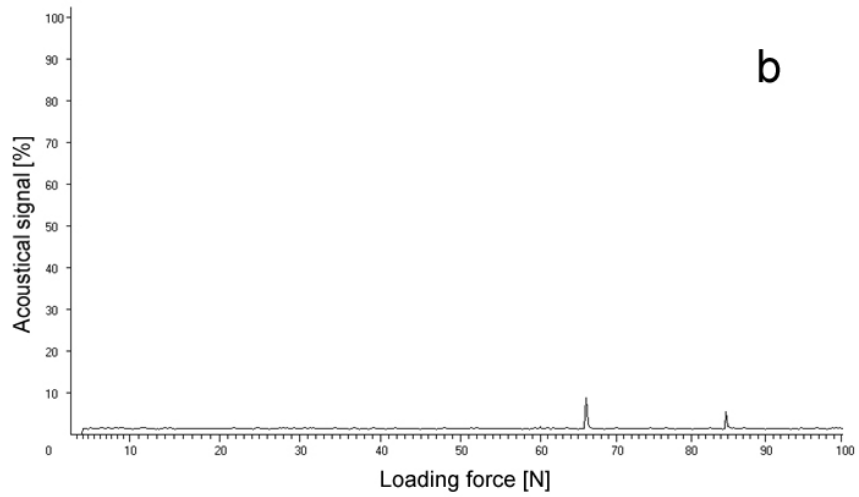
b
Acoustical signal [%]
Loading force [N]

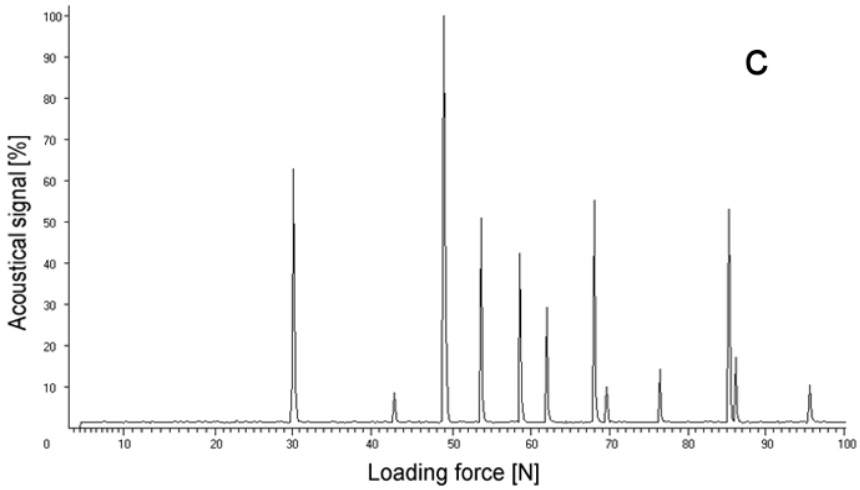
c
Acoustical signal [%]
Loading force [N]

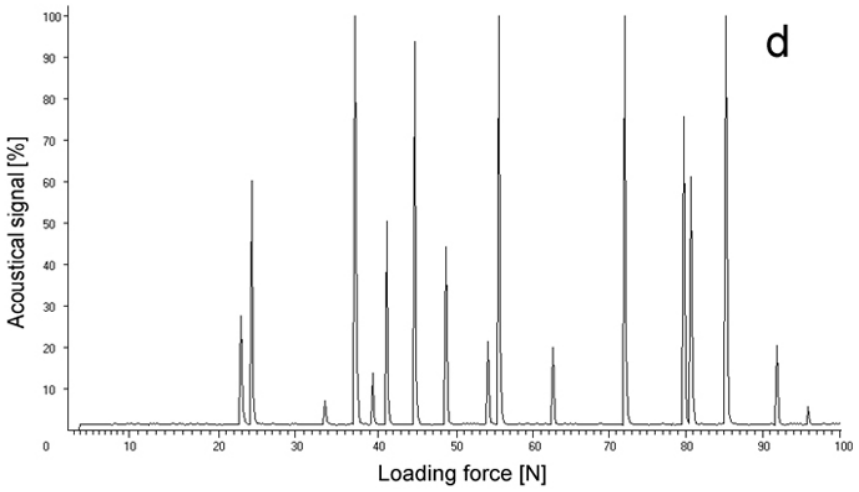
d
Acoustical signal [%]
Loading force [N]

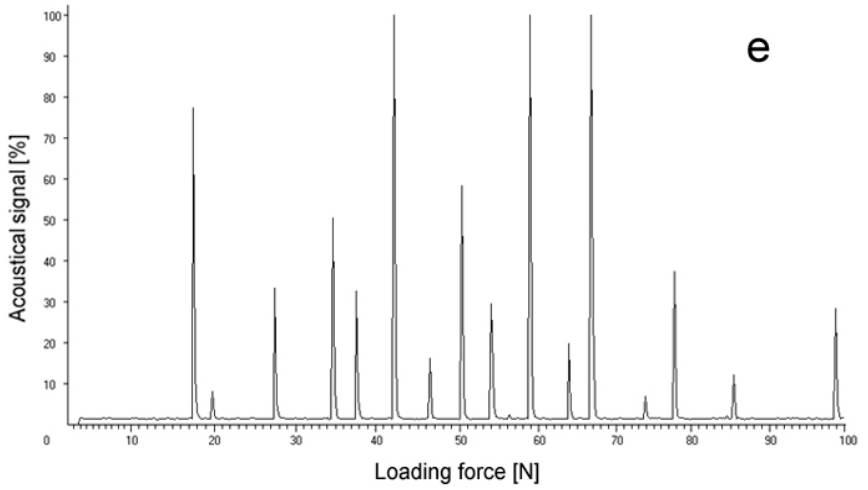
e
Acoustical signal [%]
Loading force [N]

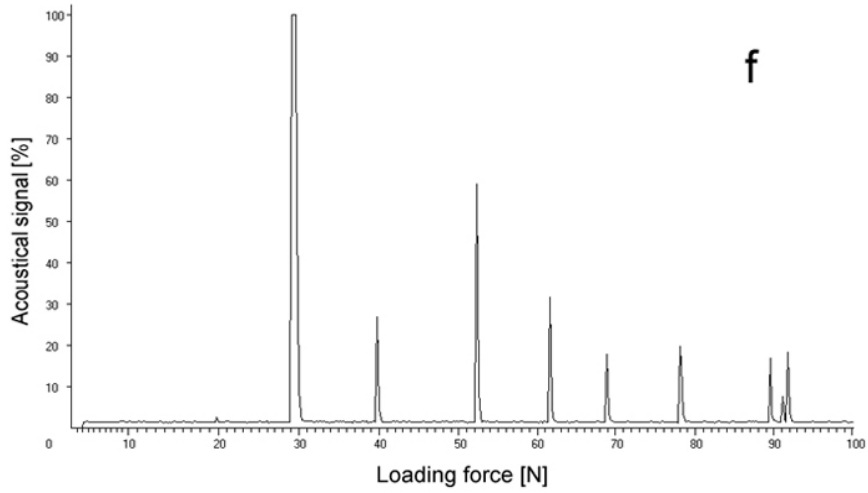
f
Acoustical signal [%]
Loading force [N]

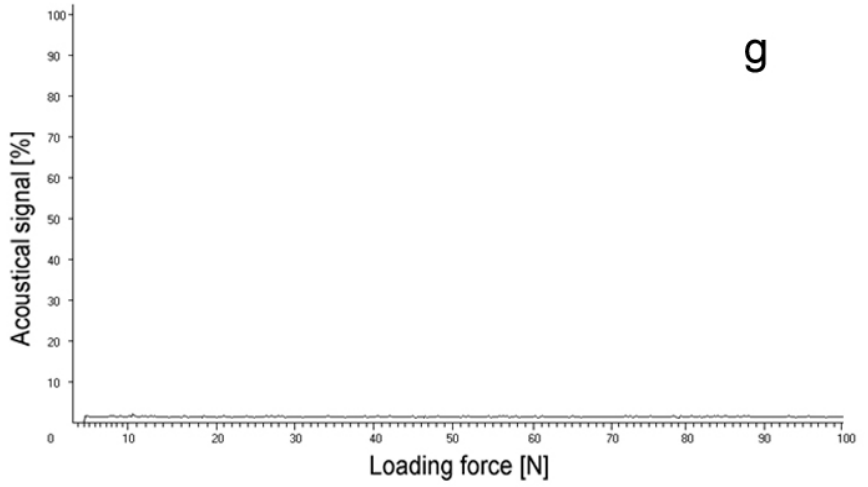
g
Acoustical signal [%]
Loading force [N]

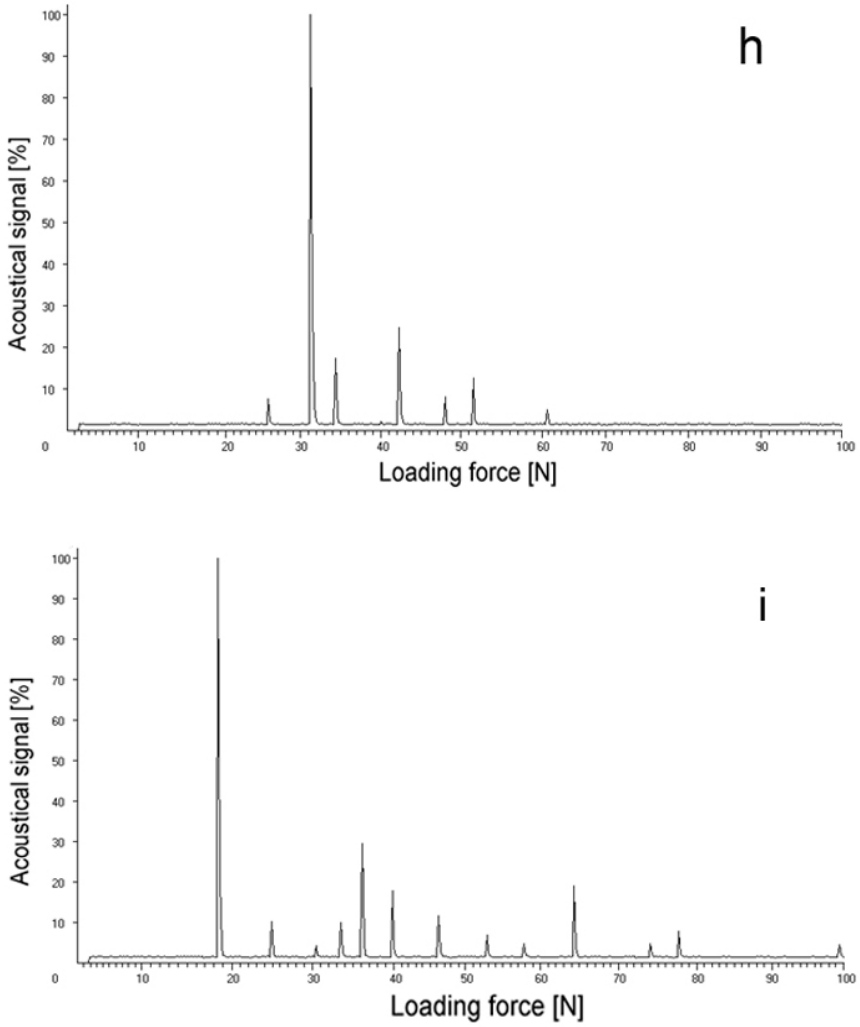

Figure S1. Representative graphs of Scratch Tests of specimens treated in different pure solvents. (a) Petroleum ether, (b) Cyclohexane, (c) Totuene, (d) n-butyl alcohol, (e) isopropyl alcohol, (f) acetone, (g) methyl alcohol, (h) DMSO, (i) H_2O.

Fig. S2 shows the cross section of TNTs in four different situations. During the Revetest Scratch Tests, the tip of needle loaded on the surface of oxide layer, induced the brittle fracture of TNTs at the proper loading force (see Figure S2 a). Fig. S2 b shows the view of TNTs' boundary after fracture, whose edge tilted and separated from the substrate. Fig. S2 c and d display the TNTs' adhesion with the substrate. Part of the oxide layer was cut and the cross section could be exposed. There exists no difference in adhesion for specimens treated in different organic solvents could be observed by SEM.

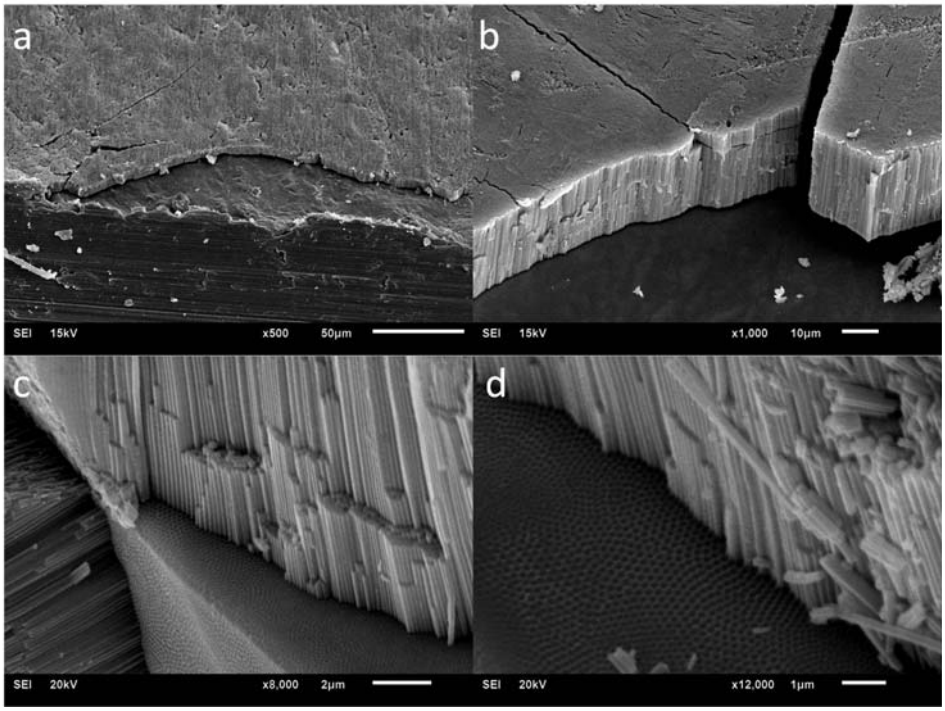

Figure S2. The cross section view of TNTs observed by SEM. (a) the fracture of TNTs caused by Revetest Scratch Tests, (b) the boundary line of TNTs after fracture, (c) TNTs treated in acetone, (d) TNTs treated in cyclohexane

2. The influences of post-treatment by organic solvents on stripping behavior of TNTs layer.

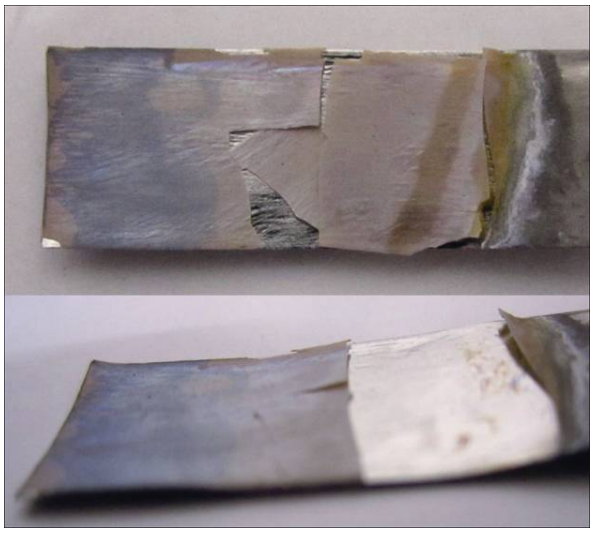

Figure S3. The influences of detachment and consolidation of different parts of the same specimens soaked in different solvents. The post-treatments by protic solvent (pure methyl alcohol, the right part stripped automatically) and aprotic solvent (pure acetone, the left part adhered on substrate tightly) can influence the adhesive strength of the tube layers to the substrate in an opposite way.

As shown in Fig. S3, it could be obviously observed that the same fabricated sample treated in different organic solvents has presented the reverse results in TNTs' adhesive strength. Views of SEM (Figure S6) showed that both the natural stripping specimen and the mechanical striping one presented the closed bottom of freestanding tube layers, however, those also indicated that the fracture interface at different point of the barrier layer of TNTs. This was consistent with the previous assumption that the barrier layer consists of two components, the inner and the outer one sharing distinguishing strength.[1]

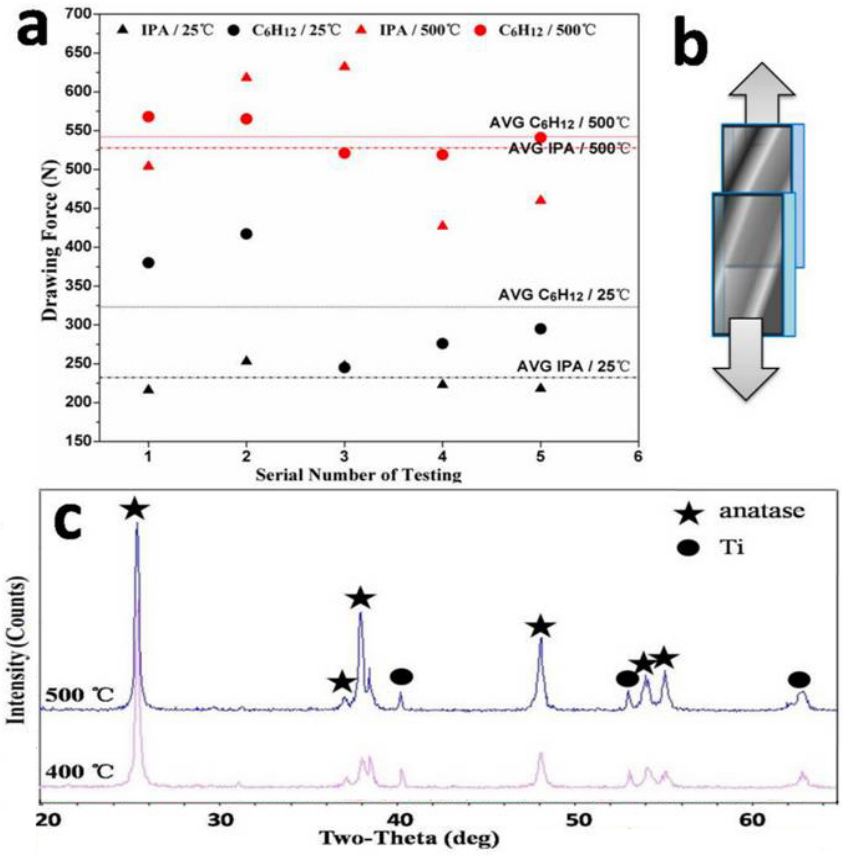

Figure S4. (a) The results of tensile tests for TNTs treated in cyclohexane (C_6H_{12}) and isopropyl alcohol (IPA); (b) the Schematic diagram of the tensile test; (c) XRD patterns for TNTs treated by 500 and 400℃ annealing for 2 hours

Here we used the fabricated TNTs after post-treatment in cyclohexane and isopropyl alcohol to explore the impact of post-treament on the annealing TNTs. Before the tensile tests, the TNTs immersed by cyclohexane and isopropyl alcohol should be divided into two groups, one group was heated at 500 ℃ for 2 hours after immersion, while the control group was dried at room temperature. Because of the phase transformation after annealing, the Revetest Scratch tests were not effective for mechanical testing of anatase TNTs. So the tensile tests were employed to characterize the TNTs' adhesion force after annealing and the designed method to characterize the adhesive force just as shown in Fig. S5b. Briefly, stick the side of TNTs to another smooth metal plate firmly and use the universal mechanical testing (system AG-IC 500N/50 KN, Shimadzu, Japan) at a tensile force rate 25N/min to draw the two sides away. With the tensile force increasing, the TNTs would ultimately delaminate from the substrate.

When the fracture occurred, the tensile forces were recorded at the moment of fracture as the reference of TNTs adhesion strength.

Specimens without annealing were taken as the controls. At the room temperature (25℃), specimens immersed by cyclohexane have presented higher adhesion than those in isopropyl alcohol (IPA), which was coincident with the results of Scratch test. However, after 500℃ annealing, specimens shared the similar adhesive strength. To our knowledge, heat treatment could be efficient to diminish the residue stress and enhance the adhesion. 2-hours annealing treatments in N2 might eliminate the differences caused by cyclohexane and isopropyl alcohol. And thus we can speculate that the limit point of the adhesion strength has turned to be the intrinsic mechanical properties of anatase TNTs rather than the fixing of barrier layer.

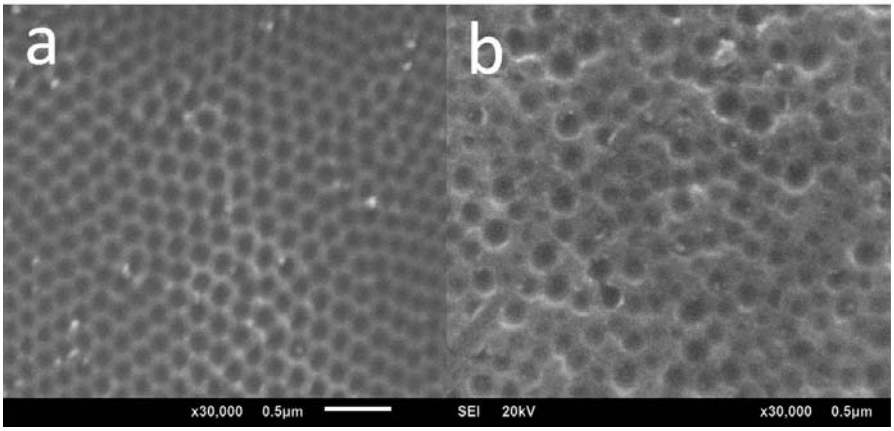

Figure S5. SEM image of Ti substrate (a) TNTs layers peeled off by natural stripping after post-treatment in the bath of pure methyl alcohol and (b) TNTs layers peeled off by mechanical stripping after post-treatment in the bath of pure cyclohexane.

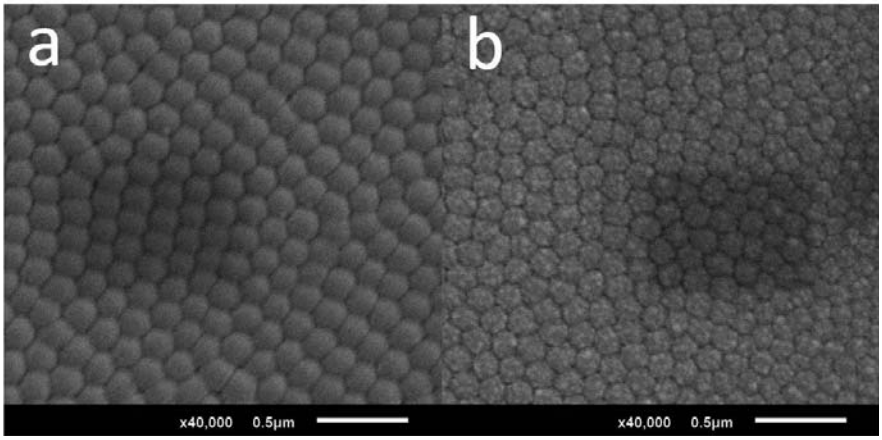

Figure S6. SEM images of bottom surface of the (a) TNTs layers peeled off by natural stripping after post-treatment in the bath of pure methyl alcohol and (b) TNTs layers peeled off by mechanical stripping after post-treatment in the bath of pure cyclohexane.

3. The double-layer micro-structure and composition of TNTs' barrier layer analyzed by XPS.

The fresh fabricated TiO_2 nanotubes specemens were immersed into the pure ethyl alcohol and dispersed them by 30 min ultrasonic washing. And then we took the ethyl alcohol mixed with the nanotubes for the preparation of the TEM test.

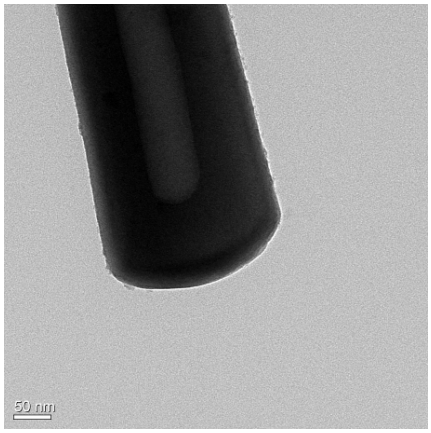

Figure S7. TEM images of single TiO_2 nanotube. Double-layers microstructure can be seen in tubes' wall and bottom.

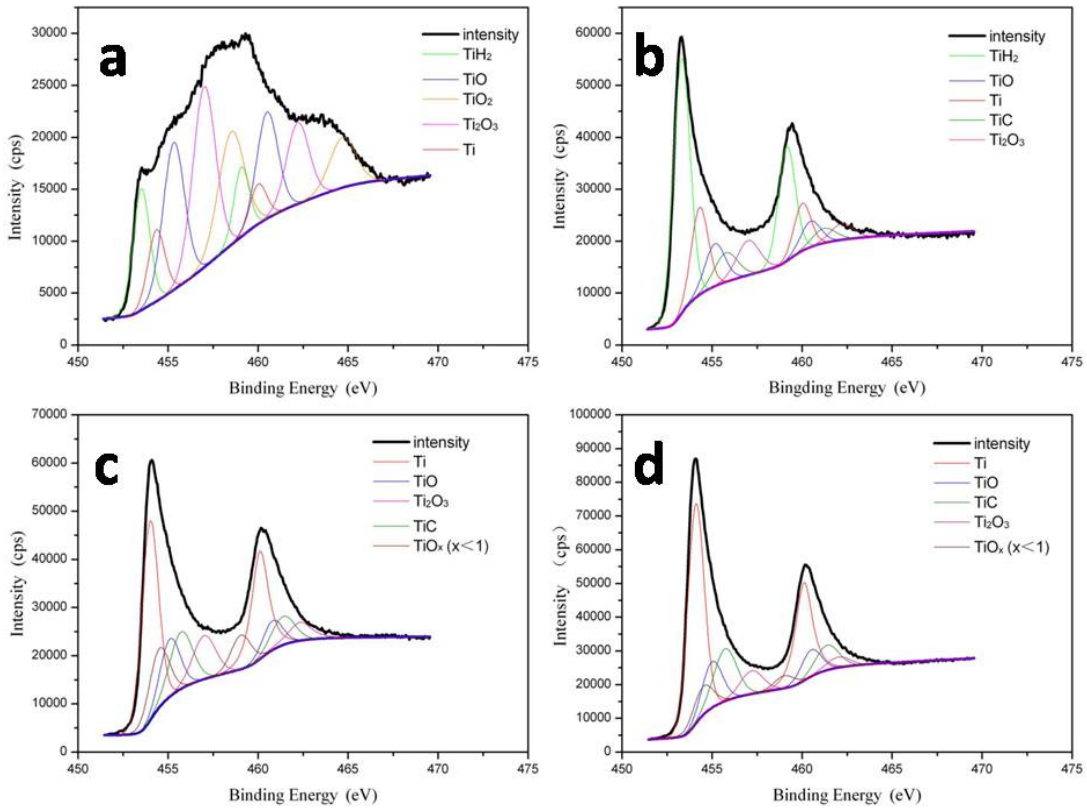

Figure S8. Phase analysis of the remaining Ti substrate after the remove of TNTs layers by XPS deeply detection: (a) substrate treated by mechanical stripping, etching layer=3, depth≈30nm; (b) the same one to (a), etching layer=7, depth≈70nm; (c) substrate treated by natural stripping, etching layer=3, depth≈30nm; (d) the same one to (c), etching layer=7, depth≈70nm.

As shown in Fig. S8 (a) and (b), TiH_2 was proposed as the major phase and turned to be more and more predominant with the deeper etching. Besides, complicated non-stoichiometric TiO_x were existence in this layer but the Ti-O ratio was reduced. Particularly, non-stoechiometric titanium dioxide presents oxygen vacancy defects[2]. So, plenty of oxygen vacancies were found existing in the superficial substrates of testing specimens. And the obvious peaks of TiO_2 (2p3/2=458.5 eV, 2p1/2=464.3 eV) in Fig. S8 (a) disappeared in Fig. S8 (b), which means the transition layer from stable phase like TiO_2 to the incomplete oxidation products formed by electrochemical anodization. However, the contrast NS specimen, shown in Fig. S8 (c) and (d), presented the relatively state phases, which mainly consisted of Ti^0.

According to the real acidic micro-environment at the bottom of TNTs during anodizing reaction, we assumed that H^+ would pass through the barrier layer and permeate into the wall and bottom of nanotubes. Therefore, these dissolved hydrogen irons and atoms would occupy the oxygen vacancies or pile into interstitial sites of cells. The positive potential of H^+ would influence the core level binding energies of titanium atoms, which could reduce the inner-orbital binding energy of Ti atoms. It is because the positive charged H^+ would attract the outer electrons of Ti, resulting in the lower density distribution of outer electron cloud. And simultaneously, the shielding effect of inner-orbital electrons would also been lowered. So, we can assume that the peaks corresponding to TiH_2 phases formed in this environment would shift to lower binding energy in XPS profiles, which is coincident with the phase analysis (Figure S8) and report of Paulin et al.[3].

According to the results of XPS, we can conclude that there is dozens of nanometer thick layer formed by non-stoichiometric TiO_x sticking on the Ti substrate. Although the O atoms is always existing both in the outer part of barrier layer and the substrate superface, both the formation of bonds and the concentration (estimated by the intensity and peak area) are distinctly different.

Except for the spectrum of Ti, the consistent inference can be concluded according to the spectra of O. In order to support the analysis of the Fig. 3, the Ti-O ratio can be figured out by the following relation. Peaks of O 1s corresponding to TiO_x ($x \leqslant 2$) range from 530.0 to 532.0 eV: when x=2, 530.0~530.2 eV; when $1.65 \leqslant x \leqslant 2$, 530.0~531.1 eV; when $1.35 \leqslant x \leqslant 1.65$, 531.1~531.3 eV; when $0.9 \leqslant x \leqslant 1.35$, 531.3~531.6 eV; when $0.73 \leqslant x \leqslant 0.9$, 531.6~531.7 eV; and the peaks at 531.9 eV, 532.0 eV represent the BBO and BOH respectively.[4-7] The results suggested that the O^{2-} was distributed in a gradient way, the concentration reduced along with the deeper etching, forming TiO_x ($0 \leqslant x \leqslant 2$), OH^- and O^{2-} could occupy the interstitial, lattice and bridge-bond sites. And these non-stoichiometry TiO_x ($0 \leqslant x \leqslant 2$) formed due to the existence of oxygen vacancy defects.

4. Acidic micro-environment of freshly fabricated TNTs and the possible location for H_2 bubbles generation.

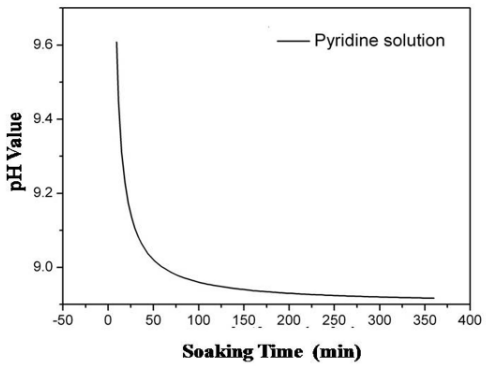

Figure S9. H^+ release process of freshly fabricated TNTs in the bath of pyridine solution.

The pH meter was used to monitor the change of pH value of pyridine solution (1M×100ml) with one freshly fabricated TNTs specimen was immersed in an enclosed and constant temperature environment. When the freshly fabricated TNTs were immersed into the bath of alkalescent pyridine solution, the electrolyte in TNTs can be renovated by the environment solution, mass of H^+ can be released into the pH monitoring pyridine solution. As shown in Fig. S9, the H^+ released very fast at first and then reached

a plateau. Therefore, it could be speculated that after about 6 hours, the nanotubular environment turned to be close to the external environment solution.

The previous studies have proposed the existence of voids between TNTs and Ti substrates, which were suggested to be the main reason of the poor adhesion strength.[8, 9] The mechanism mentioned in the manuscript is also consistent with this finding (see Figue 4 and Figure S10). The voids could become the little "storage" for H_2 gas collection.

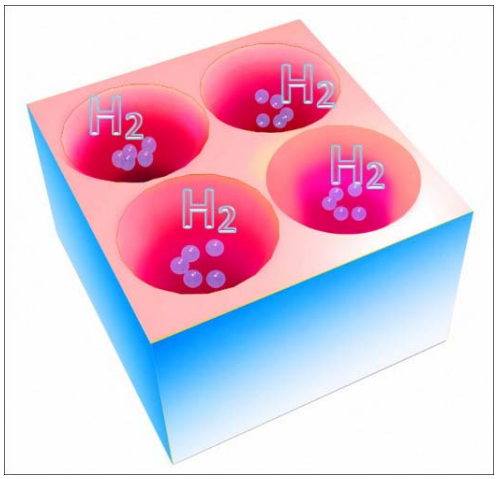

Figure S10. Schematic diagram of the possible generated H_2 molecules gathered at the interface between the barrier layer and the substrate.

REFERENCES

1. Su Z, Zhou W. Formation mechanism of porous anodic aluminium and titanium oxides. *Adv. Mater.* **20,** 3663-3667 (2008).
2. Delplancke JL, Winand R. Galvanostatic anodization of titanium—II. Reactions efficiencies and electrochemical behaviour model. *Electrochimica Acta* **33,** 1551-1559 (1988).
3. Paulin I, Donik Č, Mandrino D, Vončina M, Jenko M. Surface characterization of titanium hydride powder. *Vacuum* **86,** 608-613 (2012).
4. Takagi-Kawai M, Soma M, Onishi T, Tamaru K. The adsorption and the reaction of NH_3 and NO_x on supported V_2O_5 catalysts: effect of supporting materials. *Can. J. Chem.* **58,** 2132-2137 (1980).
5. Kuznetsov M, Zhuravlev JF, Gubanov V. XPS analysis of adsorption of oxygen molecules on the surface of Ti and TiN_x films in vacuum. *J. Electron. Spectrosc. Relat. Phenom.* **58,** 169-176 (1992).
6. Kuznetsov M, Zhuravlev JF, Zhilyaev V, Gubanov V. XPS study of the nitrides, oxides and oxynitrides of titanium. *J. Electron. Spectrosc. Relat. Phenom.* **58,** 1-9 (1992).
7. Larsson PO, Andersson A, Wallenberg L, Svensson B. Combustion of CO and toluene; characterisation of copper oxide supported on titania and activity comparisons with supported cobalt, iron, and manganese oxide. *J. Catal.* **163,** 279-293 (1996).
8. Chien-Chon C, Hsien-Wen C, Chin-Hsing C, Hsueh-Pei L, Chi-Ming L, Si-Fan C, Liyang L, Chen-Shiung H, Diau EWG. Fabrication and characterization of anodic titanium oxide nanotube arrays of controlled length for highly efficient dye-sensitized solar cells. *J. Phys. Chem. C* **112,** 19151-19157 (2008).
9. Yu D, Zhu X, Xu Z, Zhong X, Gui Q, Song Y, Zhang S, Chen X, Li D. Facile Method to Enhance the Adhesion of TiO2 Nanotube Arrays to Ti Substrate. *ACS Appl. Mat. Interfaces* **6,** 8001-8005 (2014).

5. List of abbreviations

Abbreviation	**Definition**
TNTs	TiO2 nanotubes
HAC	hydrogen-assisted cracking
DSSCs	dye-sensitized solar cells
EG	ethylene glycol
TEM	transmission electron microscopy
AFM	atomic force microscopy
XPS	X-ray photoelectron spectroscopy
DC	direct current
SEM	Scanning electron microscopy
XRD	X-ray diffraction
NS	naturally stripping
MS	mechanically stripping
BBO	bridge-bond-O
BOH	bridging –OH
F1	force due to the hydraulic pressure of the electrolyte solution
F2	forces resulting from the expansion of H_2 bubbles
F3	interfacial adhesive force
Vo	oxygen vacancies